Journal of Materials Chemistry C

Accepted Manuscript

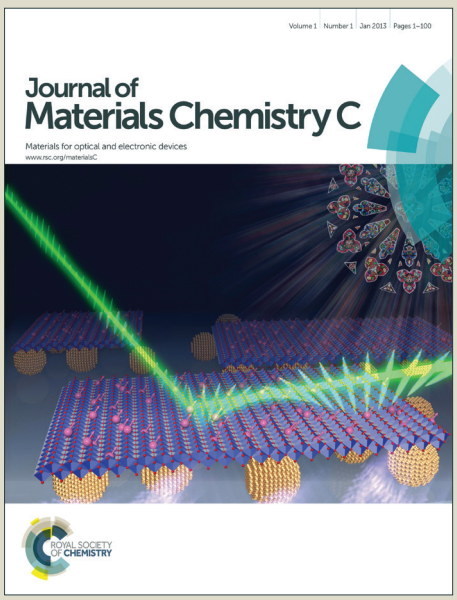

ROYAL SOCIETY OF CHEMISTRY

www.rsc.org/materialsC

The Variable Gradient Refractive Index Engineering: Design, Growth and Electro-deflective Application of $KTa_{1-x}Nb_xO_3$

Hao Tian[1*], *Peng Tan*[1], *Xiangda Meng*[1], *Chengpeng Hu*[1], *Bo Yao*[1], *Guang Shi*[1] *and Zhongxiang Zhou*[1*]

[1]Department of Physics, Harbin Institute of Technology, Harbin 150001, China

*Correspondence: H Tian, E-mail: tianhao@hit.edu.cn

Abstract

Gradient refractive index (GRIN) optical materials have received substantial attention because of their applications in integrated imaging and fiber optics. The refractive index gradient of most GRIN materials cannot be adjusted after fabrication, which limits the widespread application of GRIN materials. We propose a variable GRIN material utilizing the controllable quadratic electro-optic coefficient distribution in single crystals of $KTa_{1-x}Nb_xO_3$. By using the phase diagram of $KTa_{1-x}Nb_xO_3$, niobium composition gradient $KTa_{1-x}Nb_xO_3$ single crystals were designed and successfully grown to achieve the gradient distribution of a quadratic electro-optic coefficient by controlling growth conditions. Based on this variable, GRIN $KTa_{1-x}Nb_xO_3$, a novel high-speed electro-deflector, was produced.

Keywords: Crystal growth; Electro-optic effect; $KTa_{1-x}Nb_xO_3$; Variable gradient refractive index

Introduction

In recent decades, gradient refractive index (GRIN) optical elements have received substantial attention for their applications in integrated, imaging and fiber optics. They have properties that cannot be achieved by traditional uniform materials and simplify high-quality optical systems because their spatial distribution in the refractive index.[1,2] For instance, gradient-index lenses can enhance the focusing power of lasers and correct aberrations.[3,4] GRIN media can be created using artificially structured metamaterials because the shape and size of the structural unit of the metamaterial can be tailored, and the composition and morphology can be tuned to modify the distribution of the refractive index to provide new functionality.[5,6] Graded photonic crystal, whose refractive-index distribution can be tuned optically to control focusing and self-collimation, is also a type of GRIN media.[7]

Furthermore, variable GRIN media could change the distribution of the refractive index by exposure to an external electric field, light or other factors, resulting in more useful elements. Researches about variable GRIN media have received more and more attention. Variable GRIN has been achieved by metamaterials[8,9], and tunable liquid GRIN lens could tailor the refractive index profile by adjusting the flow conditions[10]. In addition, graded plasmonic crystals with semiconductor rods could also realize tunable GRIN optics[11]. However, methods of implementing variable GRIN materials are still difficult, which limits the applications of these media.

In 2006, NTT Photonics Laboratories implemented the application of anomalous beam deflection by employing a variable $KTa_{1-x}Nb_xO_3$ (KTN) material. In their work, the refractive index was linearly graded in KTN between the electrodes using the EO effect and the space-charge effect.[12-14] However, the space-charge effect is difficult to control in KTN when the distance between electrodes increases. The refractive index

of the electro-optic materials can be rapidly modulated by an external electric field. Some solid-solution crystals with a perovskite structure have a strong electro-optical effect.[15,16] However, research on the growth of these crystals always focuses on how to grow uniform crystals and ignores the controllable non-uniform crystals. KTN, a type of perovskite crystal, is recognized as the best electro-optic material.[17-22] In this article, we achieved the design and implementation of a variable GRIN KTN by controlling the segregation of the composition during the growth process. The variable GRIN KTN possesses a specific distribution of a quadratic electro-optic coefficient that produces variable gradient refractive index distributions under various external fields. The physical mechanisms involved in the relationship between the adjustable refractive index distribution and the composition of the gradient in KTN are explained. Using these KTN samples, a novel electro-optic deflector with a large deflection angle and a fast response speed was produced. This method could also be applied to other perovskite solid-solution crystals, which has great significance for the application and performance of functional crystal elements.

Materials and Methods

Design of variable gradient refractive index $KTa_{1-x}Nb_xO_3$ crystals

When an external electric field E is applied along the [001] direction of paraelectric $KTa_{1-x}Nb_xO_3$, the changed refractive indexes, according to the quadratic electro-optic (QEO) effect, are:

$$n_{[100]}' = n_{[010]}' \approx n_0 - \frac{1}{2} n_0^3 s_{12} E^2 \ , \ \ n_{[001]}' \approx n_0 - \frac{1}{2} n_0^3 s_{11} E^2 \qquad (1)$$

where n_0 is the refractive index when no electric field is applied and $n_{[100]}'$, $n_{[010]}'$, $n_{[001]}'$ denote the changed refractive indexes parallel to the [100], [010], and [001] axes, respectively. If the distribution of the QEO coefficients, s_{11} and s_{12}, in the crystal

could be controlled, variable gradient refractive index distributions would be realized by employing the external electric field.

The QEO coefficient s_{1j} (j = 1, 2) relates to the quadratic polarization-optic coefficient g_{1j} by:

$$s_{1j} = \varepsilon_0^{\,2} \left(\varepsilon_r - 1\right)^2 g_{1j}, \quad j = 1, 2 \tag{2}$$

where ε_0 is the vacuum permittivity and ε_r is the relative dielectric constant determined by the Curie-Weiss law in paraelectric KTN,

$$\varepsilon_r = C_1 / \left(T - T_c\right) \tag{3}$$

where T is temperature, T_c is the Curie temperature, and C_1 is a constant. Following the theory proposed by DiDomenico and Wemple, g_{1j} remains constant in all phases.[23] Furthermore, for KTN, T_c has a linear relationship with the Nb composition fraction x.[24] Hence, we can obtain the relationship

$$s_{1j} \propto \left(1/T - T_c\right)^2 = \left[1/\left(T - ax - b\right)\right]^2 \tag{4}$$

where a and b are constants for KTN crystals. Therefore, the s_{1j} distribution is related to the Nb composition distribution in KTN. If the distribution of the Nb composition fraction could be controlled, utilizing the large s_{1j} of KTN, a variable GRIN phenomenon would occur when the crystal is under the changing external electric field.

For the $KTa_{1-x}Nb_xO_3$ (KTN) grown in the $KTaO_3$-$KNbO_3$ solution, the segregation of $Nb^{5+}$and Ta^{5+} is directly impacted by growth conditions. According to the KTN phase diagram,[25] the main factors include the crystal volume (V), the raw materials' mass (M) and the growth temperature (T_g). If the growth process is in strict accordance with the phase diagram, the relationship for the main factors mentioned is:

$$V = C_2 M \Delta T_g \tag{5}$$

where C_2 is a constant and ΔT_g is the cooling rate in the growth process. Furthermore, the relationship between the Nb composition and the growth conditions could be obtained by combining the slope of the phase diagram, as shown below

$$\Delta x \propto \Delta T_g, \quad \Delta x \propto V, \quad \Delta x \propto 1/M \tag{6}$$

where Δx is the Nb composition change in the growth process. The other conditions are unchanged in our growth process, except for T_g, V and M.

High-quality crystals grown by the top-seeded solution growth (TSSG) method generally have constant diameters. Hence, the sizes of square cross-section of KTN should be controlled in the growth process. KTN morphologies have been studied by free energy models and density functional theory (DFT) calculations.[26-28] The DFT calculations, which were performed using the CASTEP code, were implemented using the plane wave basis approach.[29] The exchange correlation function was described by the Wu-Cohen generalized gradient approximation.[30] Although the proportion of Nb^{5+} and Ta^{5+} changes, the following relationship is unchanged:

$$\sigma_{110} / \sigma_{100} > \sqrt{2} \tag{7}$$

where σ_{110} and σ_{100} are the surface free energy of the (110) and (100) facets, respectively. This implies that the sectional shape would always be square by the Hartman-Perdok approach,[26] which facilitates the control of the volume. In the cooling process, the new surface energy of the solid-liquid interface could be written as:

$$\Delta G = \left(\Delta H \left(T_e - T_g\right) / T_e\right) \cdot V + \sigma_{100} \cdot \Delta A \tag{8}$$

where T_e is the equilibrium temperature, V is the grown crystal volume, ΔH is the change of enthalpy during the crystallization, and ΔA is the increased interfacial area. Only when $\Delta G < 0$, the size of square cross-section increases. Assuming that the proportion of Nb^{5+} and Ta^{5+} is 1:1, the result shows that the size of square

cross-section could not increase when 1396.3 K < T_g < T_e ≈ 1410 K. For the other proportions, T_g also has a range of values for the production of a certain size of square cross-section. Hence, when T_g is in an appropriate range, the sizes of square cross-section cannot increase even though the cooling rate is rapid. These special properties of KTN allow us to achieve specific distributions of compositions by controlling the growth temperature.

Growth of GRIN KTN

KTN single crystals were grown by the TSSG method.[31] The raw materials of K_2CO_3 (99.99%), Nb_2O_5 (99.99%) and Ta_2O_5 (99.99%) powders were weighed according to the phase diagram.[25] The mole ratio of K_2CO_3, Nb_2O_5 and Ta_2O_5 was 1.04 : 0.32 : 0.68. Then, the mixed powders were ball-milled in ethanol for 24 h. The dried mixture was placed in a platinum crucible and calcined at 900 °C for 6 h to synthesize the KTN compound. Then, the compound was melted at 1250 °C, which is higher than the temperature of crystal growth. The KTN crystal was grown on a seed in the [100] direction when the melt reached the crystallization temperature. In order to obtain appropriate sizes of square cross-section, the crystals started growth at around 1160 °C. Then the temperature was risen rapidly for keeping the size of square cross-section constant. When the crystals grew with certain sizes of square cross-section, the temperature was slowly cooled according to the temperature program until completing the growth. The curves of growth temperature are shown in Figure 1. The rotation rate remained 10 rpm and the pulling rate remained 0.3 mm/h during the growth. Finally, the as-grown crystals were cooled to the room temperature at a rate of 50 °C/h.

Properties measurement

The dielectric properties of the crystals were measured as a function of temperature at

1 kHz using an impedance-capacitance-resistance (LCR) meter (E4980A, Agilent Technologies, USA). The QEO coefficients of the polished cuboids samples were measured using a Mach-Zehnder interferometer at 25 °C.[32,33] Especially, when we measured the distributions of QEO coefficients in plane perpendicular to the pulling direction, the laser beam was expanded, spatially filtered and collimated, and the Fresnel off-axis hologram was formed and recorded on a CCD.[33] The dimensions of the KTN deflector were 4.00 mm (x) × 2.76 mm (z) × 1.60 mm (y). The z direction is the pulling direction. All surfaces were polished and the electrodes were painted on both xz faces. The deflection angles were measured under different voltages. In addition, the numerical calculation for the deflector was implemented using the finite element method (COMSOL, Inc). The response of deflection to the applied AC field was tested at frequencies up to 1.1 MHz. A slit was placed in front of the photo detector, and the output laser beam scanned across the slit, when the response was measured.[12]

Results and Discussion

Composition distribution of the variable GRIN KTN

According to the design method, a series of KTN samples with specific composition gradients was grown by the TSSG method. The as-grown crystals are shown in Figure 1a. The parameters V, M and T_g of the three crystals are controlled differently. The volume and M have been included in the legend of Figure 1a. Curves of T_g and the distribution of Nb compositions in the crystal along the growth direction are shown in Figure 1b, 1c and 1d.

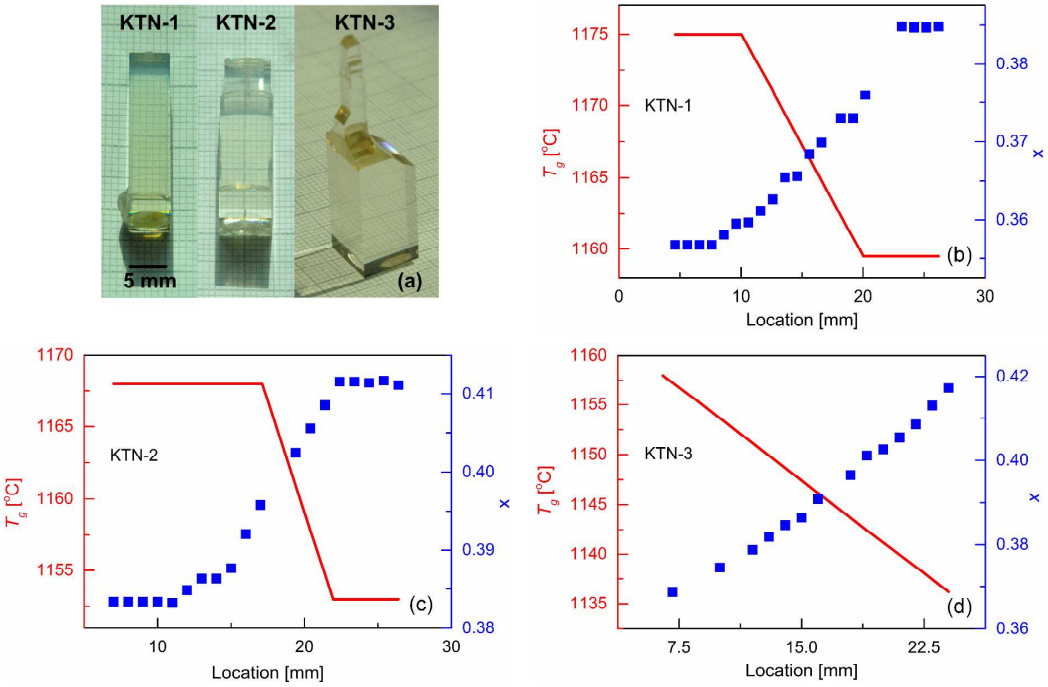

Figure 1. Photos, growth parameters and Nb compositions of the as-grown KTNs. (**a**) KTN photos. (**b**), (**c**) and (**d**) show T_g (red lines) and the distributions of x (blue dots) along the pulling direction for KTN-1, KTN-2 and KTN-3, respectively. KTN-1 employs 100 g raw materials and has a size of square cross-section of 6.05 mm × 6.05 mm and a length of 26.18 mm. KTN-2: 150 g raw materials, 7.88 mm × 7.88 mm size of square cross-section and 29.44 mm length. KTN-3: 150 g raw materials, 11.10 mm × 11.10 mm size of square cross-section and 24.50 mm length.

All three crystals have certain sizes of square cross-section under different cooling rates in the controlled temperature range, which agrees with the theoretical prediction. The growth temperature is the decisive factor for the composition segregation. The Nb compositions nearly remain constant when T_g is stable, and they increase with decreasing T_g. As the cooling rate increases, the Nb composition also increases. Furthermore, the crystals grown with large M and small V has a relatively small variation of Nb content along the growth direction, which is consistent with equation 6. In addition, the actual crystal's cross-sectional area was generally smaller than the theoretical value. From experimental results, the relationship between the segregation effect and the crystal's cross-sectional area is:

$$\frac{\Delta x_{\text{theory}}}{\Delta x_{\text{actual}}} = 0.246\frac{S_{\text{theory}}}{S_{\text{actual}}} + 0.852 \quad (9)$$

Here, S is the crystal's cross-sectional area, and the subscripts represent theoretical or actual parameters. Hence, when considering the value of S, the growth results corresponded well to the theoretical design of the variable GRIN KTN, which confirmed the feasibility of the growth method.

QEO coefficient distribution of the variable GRIN KTN

To confirm the impact of the Nb composition on the QEO coefficient distribution and to verify that the grown KTN achieved QEO coefficient distribution, the ε_r, s_{11} and s_{12} of the KTN with various x were determined. The samples were sliced along the growth direction from KTN-3. Figure 2a shows the temperature dependence of ε_r for the samples at different locations. T_c depends on location (Nb composition), and the values of ε_r are large near T_c, which will lead to a strong QEO effect. The temperature of the dashed line in Figure 2a is 25 °C, at which the QEO coefficient measurements were conducted. The results are shown in Figure 2b. The ε_r of different locations formed a gradient (Figure 2b inset) and caused a gradient distribution of s_{1j}. The red, dashed line shows the fitting results of the s_{1j} distribution obtained from equation 4. The samples have large QEO coefficients that reach 1.04×10^{-14} m^2V^{-2} for the samples with a T_c of 25 °C. In addition, the distributions of the QEO coefficients on the plane perpendicular to the pulling direction are relatively uniform (Figure 2c) as a result of the appropriate rotation rate of growth that we chose. The distribution of the QEO coefficient is controlled only along the growth direction. Based on the results above, the distribution of large QEO coefficients has been achieved according to equation 4, which verifies the validity of the design method again. The refractive index was measured by an ellipsometer when there was no external electric field. The refractive

index distributions under different electric field were calculated by equation 1 according to the fitting relation curve of QEO coefficients and locations, and are shown in Figure 3. The white and light gray regions are paraelectric under 25 °C. The refractive index distribution along the crystal growth direction varied with the external field. Hence, the designed KTN could enable the production of variable GRIN elements under a variable external electric field.

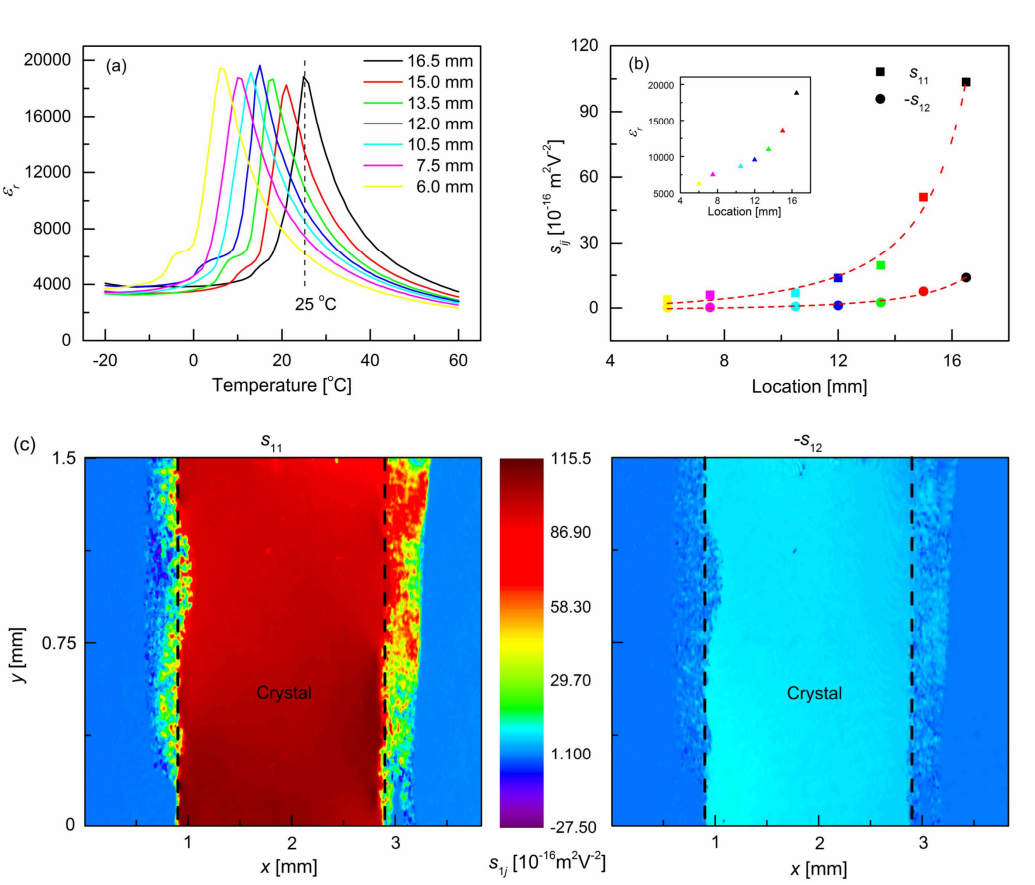

Figure 2. Temperature dependence of ε_r and the distributions of QEO coefficients of the sample from KTN-3 at 25 °C. (**a**) ε_r vs. temperature. (**b**) Distributions of s_{11} and s_{12} along the pulling direction. The red dashed line shows the fitting results from equation 4. The inset figure shows the ε_r distribution. (**c**) The distributions of s_{11} and s_{12} in the face perpendicular to the pulling direction at the 16.5 mm location of the sample at 25 °C.

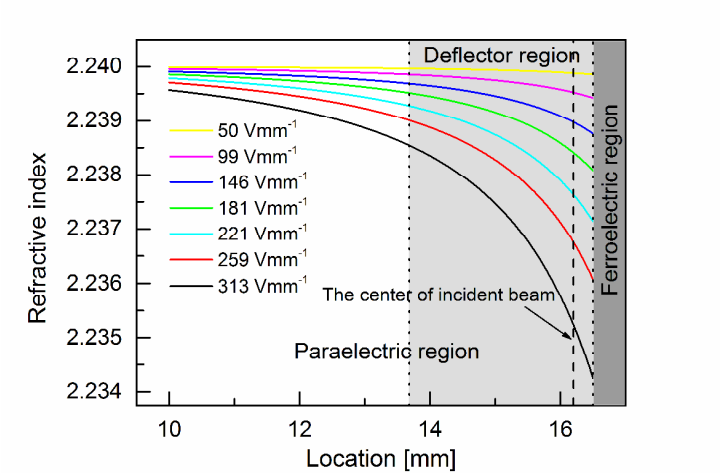

Figure 3. The calculated distributions of refractive index of KTN-3 at 25 °C under different external electric field. The white and light gray regions are paraelectric, and the dark gray region is ferroelectric. The deflector was cut from the light gray region.

The Electro-deflective application

The natural fast response properties of the EO effect and the large QEO coefficients of KTN make it possible to realize a high speed and a large scanner angle for the electro-deflector. For the KTN sample that is schematically illustrated in Figure 4a, the z direction is the pulling direction and the variation of s_{ij} is along the z direction. As a laser beam (polarized parallel to the electric field) propagates through the crystal, the change of the refractive index along the z direction ($\Delta n(z)$) under the external electric field is:

$$\Delta n(z) = -\frac{1}{2} n_0^3 s_{11}(z) E^2 \tag{10}$$

where $s_{11}(z)$ is the QEO coefficient and it changes with z. The deflection angle θ at the export is:

$$\theta = l\left|\frac{d\Delta n}{dz}\right| = \frac{1}{2} n_0^3 E^2 l \left|\frac{ds_{11}(z)}{dz}\right| \tag{11}$$

where $ds_{11}(z)/dz$ represents the gradient of s_{11} along the z direction, and l is the length

of the crystal along the x direction. The deflection angle was determined by the s_{11} change along z.

The rectangular KTN sample (4.00 mm (x) × 2.76 mm (z) × 1.60 mm (y)) was cut from KTN-3. The location of incident beam is shown in Figure 3, the refractive index gradient is about 2.65 × 10^{-3} mm^{-1} around this site under an electric field of 313 Vmm^{-1}. The theoretical, numerical and experimental results of deflection angles under different applied voltages are shown in Figure 4b. The three results were consistent with each other. The EO deflector generates a large deflection angle of 0.61° at a low applied electric field of 313 Vmm^{-1}, compared with Ref. (12). Furthermore, the response of this electro-deflector is fast with a scan frequency up to 2.2 MHz (Figure 4c). Therefore, this KTN is suitable for fast modulation of light, which offers a great advantage compared to similar products.[12-14]

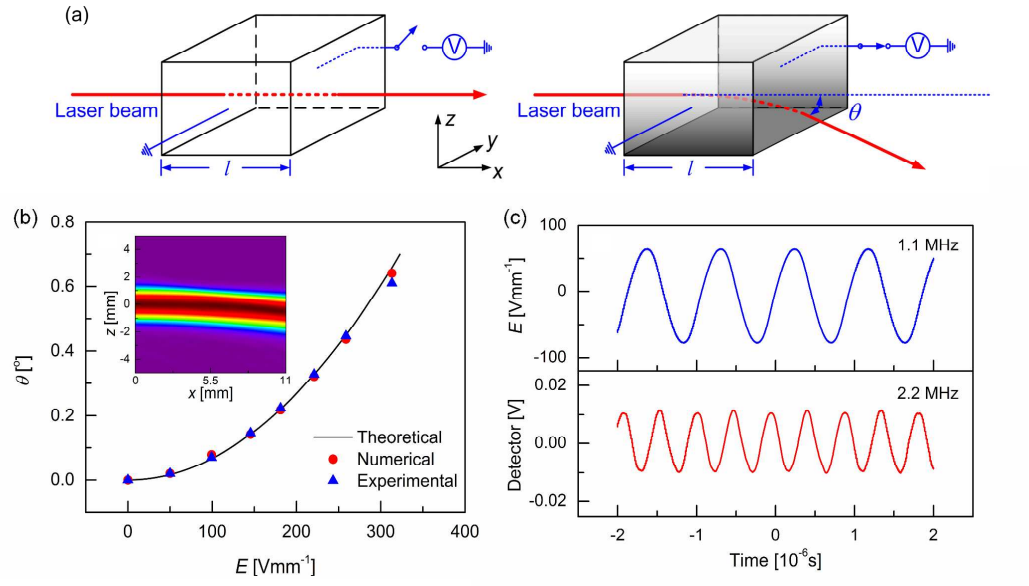

Figure 4. The deflector fabricated by the variable GRIN KTN. (**a**) Schematic diagram for the electro-deflector. The incident light, which was polarized along the applied electric field, propagated along the x direction. (**b**) Deflection angles of theoretical, numerical and experimental results at various applied voltages. The inset figure shows the numerical deflection track when the applied electric field is 800 Vmm^{-1}. (**c**) The response of the deflector.

Conclusion

Based on the variable GRIN KTN design method, KTN with a specific distribution of EO coefficients has been grown by controlling the distribution of compositions. The compositions are controlled by adjusting T_g, V and M in the KTN growth process. The experimental results confirm the validity of our method for design and growth of the variable GRIN KTN and imply that this method is a viable way to implement GRIN materials. Furthermore, a novel EO deflector that has large deflection angles and a quick response time was designed and fabricated. The novel GRIN KTN crystals obtained have large QEO coefficients (s_{11} could reach $1.04\times10^{-14}m^2V^{-2}$), a rapid response speed of 2.2 MHz, and good optical quality. Moreover, as a result of the QEO coefficient distribution, the variable GRIN in KTN could be achieved, and it could be employed in optical communication to achieve large continuous deflections and high-speed electro-optic modulation. Hence, the variable GRIN KTN crystals have significant potential for the development of EO elements. In addition, the method of growing the GRIN KTN crystals might also be suitable for other perovskite crystals. Therefore, more types of variable GRIN materials with specific distributions of certain performances could be implemented, which is of great value for designing and manufacturing novel crystal functional devices.

Acknowledgements

This work was supported by the National Natural Science Foundation of China (Grant Nos. 50902034, 11074059 and 61205011), the Science Fund for Distinguished Young Scholars of Heilongjiang Province (Grant No. JC200710), and the Program for Innovation Research of Science in Harbin Institute of Technology. The authors wish to thank the Laboratory of Micro-Optics and Photonic Technology of Heilongjiang Province for help with the experiments.

Reference

1 S. Larouche, Y. Tsai, T. Tyler, N. M. Jolerst, D. R. Smith, *Nat. Mater.*, 2012, **11**, 450-454.

2 A. K. Yakhkind, *J. Opt. Technol.*, 2003, **70**, 877-881.

3 Y. Jin, H. Tai, A. Hiltner, E. Baer, J. S. Shirk, *J. Appl. Polym. Sci.*, 2007, **103**, 1834-1841.

4 J. M. Gordon, *Appl. Optics*, 2000, **39**, 3825-3832.

5 V. M. Shalaev, *Science*, 2008, **322**, 384-386.

6 R. Liu, C. Ji, J. J. Mock, J. Y. Chin, T. J. Cui, D. R. Smith, *Science*, 2009, **323**, 366-369.

7 H. Kurt, D. S. Citrin, *Opt. Express*, 2007, **15**, 1240-1253.

8 M. D. Goldflam, T. Driscoll, B. Chapler, O. Khatib, N. M. Jokerst, S. Palit, D. R. Smith, B. Kim, G. Seo, H. Kim, M. D. Ventra, D. N. Basov, *Appl. Phys. Lett.*, 2011, **99**, 044103.

9 I. E. Khodasevych, I. V. Shadrivov, D. A. Powell, W. S. T. Rowe, A. Mitchell, *Appl. Phys. Lett.*, 2013, **102**, 031904.

10 X. Mao, S. S. Lin, M. I. Lapsley, J. Shi, B. K. Juluri, T. J. Huang, *Lab Chip*, 2009, **9**, 2050-2058.

11 B. Vasić, R. Gajić, *J. Opt. Soc. Am. B*, 2012, **29**, 79-87.

12 L. Tian, D. A. Scrymgeour, A. Sharan, V. Gopalan, *Appl. Phys. Lett.*, 2003, **83**, 4375-4377.

13 K. Nakamura, J. Miyazu, M. Sasaura, K. Fujiura, *Appl. Phys. Lett.*, 2006, **89**, 131115.

14 K. Nakamura, J. Miyazu, Y. Sasaki, T. Imai, M. Sasaura, K. Fujiura, *J. Appl. Phys.*, 2008, **104**, 013105.

15 Y. Lin, B. Ren, X. Zhao, D. Zhou, J. Chen, X. Li, H. Xu, D. Lin, H. Luo, *J. Alloy. Compd.*, 2010, **507**, 425-428.

16 Y. Chang, C. Wang, S. Yin, R. Hoffman, A. Mott, *Opt. Lett.*, 2013, **38**, 4574-4577.

17 E. DelRe, F. D. Mei, J. Parravicini, G. Parravicini, A. J. Agranat, C. Conti, *Nat. Photonics*, 2015, **9**, 228-232.

18 H. Harutyunyan, *Nat. Photonics*, 2015, **9**, 213-214.

19 H. Tian, B. Yao, C. Hu, X. Meng, Z. Zhou, *Appl. Phys. Express*, 2014, **7**, 062601.

20 Z. Zhou, Y. Du, C. Hou, H. Tian, Y. Wang, *J. Opt. Soc. Am. B*, 2011, **28**, 1583-1590.

21 L. Li, Z. Zhou, H. Tian, D. Gong, Z. Yang, Y. Yang, *J. Appl. Phys.*, 2010, **108**, 043520.

22 K. Zhan, C. Hou, H. Tian, Y. Zhang, *Phys. Lett. A*, 2010, **374**, 1242-1245.

23 S. H. Wemple, M. DiDomenico, *J. Appl. Phys.*, 1969, **40**, 735-752.

24 T. Sakamoto, M. Sasaura, S. Yagi, K. Fujiura, Y. Cho, *Appl. Phys. Express*, 2008, **1**, 101601.

25 A. Reisman, S. Triebwasser, F. Holtzberg, *J. Am. Chem. Soc.*, 1955, **77**, 4228-4230.

26 D. Winn, M. F. Doherty, *AIChE J.*, 2000, **46**, 1348-1367.

27 R. I. Eglitis, D. Vanderbilt, *Phys. Rev. B*, 2008, **77**, 195408.

28 Y. Song, Z. Guo, R. Yang, *Phys. Rev. B*, 2004, **69**, 094205.

29 S. J. Clark, M. D. Segall, C. J. Pickard, P. J. Hasnip, M. I. J. Probert, K. Refson, M. C. Payne, *Z. Kristallogr.*, 2005, **220**, 567-570.

30 Z. Wu, R. E. Cohen, *Phys. Rev. B*, 2006, **73**, 235116.

31 H. Tian, Z. Zhou, D. Gong, H. Wang, D. Liu, Y. Jiang, *Appl. Phys. B*, 2008, **91**, 75-78.

32 Y. Lu, Z. Cheng, S. E. Park, S. Liu, Q. Zhang, *Jpn. J. Appl. Phys.*, 2000, **39**, 141-145.

33 Q. Lv, S. Zhao, H. Dai, Y. Zhang, *IEEE Photonics J.*, 2014, **6**, 2600110.

Table of Content

The variable gradient refractive index material is proposed utilizing the controllable quadratic electro-optic coefficient distribution in single crystals of $KTa_{1-x}Nb_xO_3$.